Evaluating the representation of tropical stratocumulus and shallow cumulus clouds as well as their radiative effects in CMIP6 models using satellite observations

Nina Črnivec[1,2], Grégory Cesana[1,2], Robert Pincus[3]

[1]Center for Climate Systems Research, Columbia University, New York, NY, USA
[2]NASA Goddard Institute for Space Studies, New York, NY, USA
[3]Lamont-Doherty Earth Observatory, Columbia University, Palisades, NY, USA

Key Points:

- We introduce a new approach to distinguish stratocumulus and shallow cumulus regimes over tropical oceans based on cloud cover.
- The 'too-few, too bright' tropical low-cloud problem persists in twelve CMIP6 models within stratocumulus and shallow cumulus regimes.
- Most CMIP6 models underestimate (overestimate) the relative frequency of occurrence of stratocumulus (shallow cumulus).

Corresponding author: Nina Črnivec, `nina.crnivec@nasa.gov`

Abstract

Low clouds over tropical oceans reflect a great proportion of solar radiation back to space and thereby cool the Earth, yet this phenomenon has been poorly simulated in several previous generations of climate models. The principal aim of the present study is to employ satellite observations to evaluate the representation of marine tropical low clouds and their radiative effect at the top of the atmosphere in a subset of latest climate models participating in CMIP6. We strive for regime-oriented model validation and hence introduce a qualitative approach to discriminate stratocumulus (Sc) from shallow cumulus (Cu). The novel Sc-Cu categorization has a conceptual advantage of being based on cloud properties, rather than relying on a model response to a cloud-controlling factor. We find that CMIP6 models underestimate low-cloud cover in both Sc- and Cu-regions of tropical oceans. A more detailed investigation of cloud biases reveals that most CMIP6 models underestimate the relative frequency of occurrence (RFO) of Sc and overestimate RFO of Cu. We further demonstrate that tropical low cloudiness in CMIP6 models remains too bright. The regime-oriented validation represents the basis for improving parameterizations of physical processes that determine the cloud cover and radiative impact of Sc and Cu, which are still misrepresented in current climate models.

Plain Language Summary

Similar as white snow and ice caps, bright low clouds have a high shortwave albedo, reflecting a huge amount of sunlight back to space and thereby helping us counteract global warming. The shadowing effect of bright low clouds is especially pronounced over tropical oceans, since equatorial regions of our planet receive most sunshine, which is in clear skies otherwise practically entirely absorbed within the contrastingly dark ocean. Climate models had traditionally struggled simulating these clouds by underestimating their areal extent and simultaneously overestimating their reflectivity. In other words, simulated clouds were commonly found to be 'too few' and 'too bright' compared to observations, which introduced a substantial uncertainty to climate projections. Herein we proposed a novel approach to proficiently decompose tropical low cloudiness into stratocumulus and shallow cumulus regime, which is essential to provide a proper guidance for climate model development. We subsequently showed that the newest generation of climate models still suffers from the 'too few, too bright' tropical low cloud problem within both stratocumulus and shallow cumulus regimes, which thus needs to be further tackled with the greatest possible endeavor.

1 Introduction

Bright low clouds cover substantial areas of dark tropical oceans and play a critical role in regulating the Earth's radiative energy budget (Bony and Dufresne, 2005; Schneider et al., 2017; Cesana and Del Genio, 2021). They reflect a substantial portion of the incoming sunlight back to space and thus exert a profound cooling effect on the Earth's climate. Climate models, however, have a longstanding problem simulating these clouds, which limits our ability to accurately predict the amount of global warming caused by rising greenhouse gas emissions (Bony and Dufresne, 2005; Sherwood et al., 2020).

A major issue, which persisted in previous generations of climate models of the World Climate Research Programme's Coupled Model Intercomparison Project (CMIP), is known as the 'too-few, too bright' tropical low-cloud problem (Nam et al., 2012). In brief, climate models commonly underestimated the amount of tropical and subtropical low-level clouds (e.g., Teixeira et al. 2011; Cesana and Chepfer, 2012; Cesana and Waliser, 2016; Cesana et al., 2019c) and simultaneously overestimated their reflectance (e.g., Weare, 2004; Karlsson et al., 2008; Nam et al., 2012). In the present study we revisit the 'too-few, too bright' tropical low-cloud problem in latest climate models participating in phase

6 of CMIP (CMIP6; Eyring et al., 2016), which are currently being evaluated as a community effort (Schuddeboom and McDonald, 2021; Tselioudis et al., 2021).

Satellite observations have been regularly exploited to assess the fidelity of climate models (e.g., Pincus et al., 2008; Jiang et al., 2012; Cesana and Chepfer, 2012; Cesana et al., 2019c), being especially valuable due to their extensive coverage. Evaluating clouds (and other fields) simulated by global climate models (GCMs) using satellite observations, however, is challenging, because satellite-borne instruments do not directly measure meteorological quantities of interest as simulated by GCMs. In order to facilitate the comparison between observed and model-simulated fields, the Cloud Feedback Model Intercomparison Project (CFMIP) community introduced the CFMIP Observation Simulator Package (COSP; Bodas-Salcedo, 2011; Swales et al., 2018). Given the atmospheric data provided by a GCM, the COSP software reproduces observations of multiple instruments on board of various satellite missions such as CloudSat (Stephens et al., 2002) and Cloud-Aerosols Lidar and Infrared Pathfinder Satellite Observations (CALIPSO; Winker et al., 2010) within the A-train constellation (Stephens et al., 2002, 2018).

To summarize, the objective of the present study is to employ satellite observations to evaluate tropical low clouds together with their radiative effect at the top of the atmosphere (TOA) in a subset of CMIP6 models. In particular, we strive to assess model representation of individual low-cloud regimes commonly found in tropical areas of large-scale subsidence − namely the eastern ocean stratocumulus (Sc) and trade wind shallow cumulus (Cu). These essentially contrasting cloud types are driven by a distinct interplay of small-scale processes within the moist marine boundary layer − convection, turbulence, radiation and cloud microphysics (Ackerman et al., 1993, 2000, 2009; Ackerman and Toon, 1996; Stevens et al., 2001), which are often poorly and inconsistently parameterized across climate models (Randall et al., 2003; Stevens and Bony, 2013; Bony et al., 2015; Klein et al., 2017). A cloud-regime-oriented model evaluation would help identify shortcomings of physical parameterization schemes, which govern the formation and evolution of Sc and Cu clouds, and is thus a crucial first step towards more reliable climate change projections. Furthermore, Sc and Cu clouds exhibit a fundamentally contrasting response to the change in their controlling meteorological factors such as rising sea surface temperature and low-level inversion strength and are associated with different feedbacks (Cesana and Del Genio, 2021), which highlights the importance of a regime-based investigation. Accurate representation of geographical distributions of Sc and Cu clouds is thereby essential for realistic low-cloud feedbacks (Cesana and Del Genio, 2021).

To carry out such a cloud regime-oriented evaluation of climate models, however, one has to find a qualitative way to separate Sc from Cu, because CMIP diagnostics do not distinguish between stratiform and convective cloud covers. A classic way to separate Sc from Cu clouds in tropical and subtropical areas of large-scale subsidence is by means of the estimated inversion strength (EIS), which is known to be a good predictor of stratocumulus (Wood and Bretherton, 2006). Even though this approach generally works well in the real world, it has limitations when applied to climate models which misrepresent EIS. An important aim of the present work is to introduce a novel Sc-Cu categorization, which can be utilized to reliably separate contributions from Sc and Cu clouds in both observations and climate models.

The remainder of this paper is structured as follows. Section 2 presents observational, reanalysis and CMIP6 data as well as various approaches to discriminate Sc from Cu. The evaluation of climate models using the Sc-Cu categorization introduced in this study is carried out in Section 3. A brief summary and concluding remarks are given in Section 4.

2 Data and Methods

2.1 Satellite observations and reanalysis data

We utilize low-cloud cover (LCC) observations from the GCM-Oriented CALIPSO Cloud Product version 2.9 (CALIPSO-GOCCP; Chepfer et al., 2010, Cesana et al., 2016), which was specifically designed to evaluate cloudiness simulated by GCMs using a lidar simulator. It is based on measurements taken by the CALIPSO Cloud-Aerosol Lidar with Orthogonal Polarization (CALIOP, Winker et al., 2010). We restrict our analysis to subsidence regimes over tropical and subtropical oceans (between 35S and 35N), where the pressure vertical velocity at 500 hPa exceeds 10 hPa day^{-1}. In these regions the amount of high-cloud is small and hence generates less attenuation of the lidar signal, thereby reducing the high-cloud shielding effect.

To discriminate Sc from Cu we use the recently created Cumulus And Stratocumulus CloudSat-CALIPSO Dataset (CASCCAD) described in detail by Cesana et al. (2019b). This unique algorithm considers cloud morphology to classify low cloudiness into several categories including Sc, Cu and various transitioning regimes (broken Sc, Cu under Sc, and Cu with stratiform outflow) at the orbital level. CASCCAD reports monthly values of cloud fraction over a 10-year period (2007−2017) and has a spatial resolution of 2.5 degrees in both latitudinal and longitudinal directions.

The observed cloud-radiative effect (CRE) estimates at TOA are obtained from the Clouds and the Earth's Radiant Energy System (CERES) Energy Balanced and Filled (EBAF) satellite product Ed. 4.1 (Loeb et al., 2018). Specifically, the CERES-EBAF clear-sky and all-sky radiative fluxes are employed to compute the CRE. We consider solely the short-wave (SW) CRE component, since low clouds contribute minorly to the long-wave TOA radiation budget.

The middle-tropospheric pressure vertical velocity at 500 hPa, which is used to define the subsidence regimes, is derived from averaging three reanalysis datasets including Modern-Era Retrospective Analysis for Research and Applications version 2 (MERRA-2), the fifth generation of ECMWF reanalysis (ERA-5) and the NCEP Department of Energy Atmospheric Model Intercomparison Project reanalysis (NCEP-DOE R-2). The same three reanalysis datasets are employed to compute EIS. All data were regridded to the CASCCAD spatial grid.

2.2 Climate models

We analyze monthly mean output of CMIP6 climate model experiments, which relate to the Atmospheric Model Intercomparison Project (AMIP) using a prescribed sea surface temperature. The CALIPSO lidar simulator (Chepfer et al., 2008) integrated in COSP is employed to consistently compare low cloudiness in observations and climate models. We investigate the realism of 12 model configurations stemming from different modeling centers given in Table 1, which provided the output of CALIPSO lidar simulator. To address the atmospheric variability within a vast GCM grid column, the COSP instrument simulator operates on a multitude of homogeneous subcolumns to reproduce satellite pixel variability. These subcolumns are normally produced within COSP in accordance with GCM's assumptions for subgrid cloud structure utilizing the Subgrid Cloud Overlap Profile Sampler (Webb et al., 2001). A few GCMs from the analyzed set employ COSP2 (Swales et al., 2018), whereby subcolumns can be adopted directly from a GCM, since they are often stochastically generated (Räisänen et al., 2004) within model's radiation scheme such as the commonly employed McICA algorithm (Pincus et al., 2003).

We employ 8 years of CMIP6 simulations (2007−2014), which overlap with the CASCCAD temporal range and regrid them to the observational spatial grid.

Model acronym	Modeling center	Reference
NorESM2-LM	Norwegian Climate Center, Norway	Seland et al. (2020)
MIROC6	Center for Climate System Research, Japan	Tatebe et al. (2019)
GISS-E2-1-G	NASA Goddard Institute for Space Studies, USA	Kelley et al. (2020)
BCC-CSM2-MR	Beijing Climate Center, China	Wu et al. (2019)
MRI-ESM2-0	Meteorological Research Institute, Japan	Yukimoto et al. (2019)
GFDL-CM4	NOAA Geophysical Fluid Dynamics Laboratory, USA	Held et al. (2019)
IPSL-CM6A-LR	Institute Pierre Simon Laplace, France	Boucher et al. (2020)
CNRM-CM6-1	National Centre for Meteorological Research, France	Voldoire et al. (2019)
CESM2	National Center for Atmospheric Research, USA	Danabasoglu et al. (2020)
E3SM-1-0	US Department of Energy, USA	Golaz et al. (2019)
HadGEM3-GC31-LL	Met Office Hadley Centre, UK	Andrews et al. (2020)
CanESM5	Centre for Climate Modeling and Analysis, Canada	Swart et al. (2019)

Table 1. List of analyzed CMIP6 models.

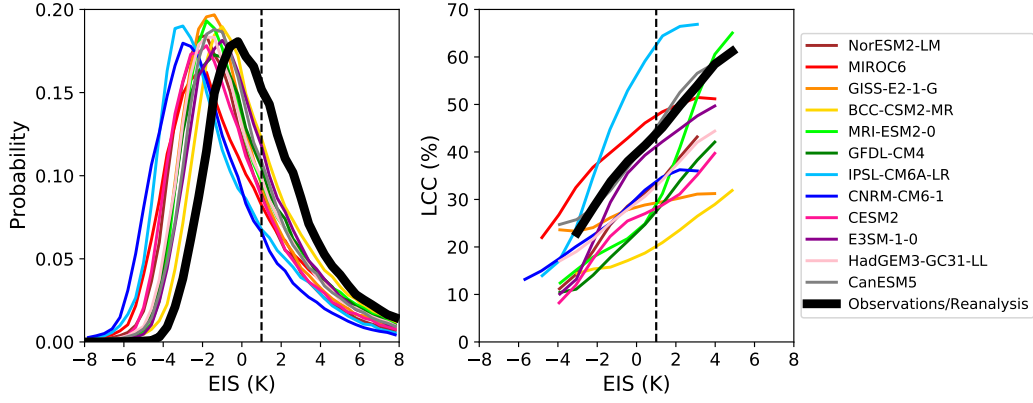### 2.3 Approaches to discriminate Sc from Cu

As pointed out in the Introduction it is challenging to evaluate the representation of Sc and Cu in climate model output, since only a single low-cloud cover variable is archived in the CMIP database. In the following we first summarize the traditional approach to separate Sc from Cu based on environmental characteristics and subsequently present an alternative, new categorization.

2.3.1 Categorization based on EIS

A traditional approach to differentiate between individual low-cloud regimes in tropical and subtropical areas governed by large-scale subsidence is by means of some measure of lower-tropospheric stability (e.g., Nam et al., 2012; Myers et al., 2021), since regions of the main stratocumulus decks off the west coast of the continents are associated with stronger atmospheric stability than shallow cumulus areas in the trade winds. A convenient parameter to describe low-level atmospheric stability is the estimated inversion strength (Wood and Bretherton, 2006) and an EIS threshold of 1 K − despite being imperfect (Cesana and Del Genio, 2021) − was commonly employed in previous work to determine whether (model) grid box is classified as being either Sc- or Cu-dominated (e.g., Myers et al., 2021).

This categorization has additional shortcomings when applied to climate models. Figure 1 (left) shows probability density of EIS in averaged renalysis (combining MERRA-2, ERA-5, NCEP data) and CMIP6 models. All analyzed models systematically underestimate EIS implied by reanalyses, although they relatively well capture the shape of the EIS distribution. This large underestimation of EIS in CMIP6 models implies that the traditional Sc-Cu categorization utilizing a fixed EIS threshold of 1 K tends to allocate an insufficient amount of LCC to the Sc component, while attributing an excessive amount of LCC to the Cu component in models.

Figure 1 (right) additionally visualizes LCC as a function of EIS derived from observations/reanalyses and CMIP6 models. Observed LCC increases with an approximately constant rate of about 5 % per K of EIS rise. Models have a differing ability to reproduce the rate of this increase, whereby multiple models strongly misrepresent the LCC-EIS relationship, making EIS not the ideal choice for discriminating among cloud types.

Figure 1. Left: Probability density functions of estimated inversion strength in subsidence regimes of tropical oceans derived from reanalyses and CMIP6 models. Right: Relationship between LCC and EIS in observations/reanalyses and CMIP6 models. The vertical dashed line at EIS of 1 K marks the common threshold used to discriminate Sc from Cu.
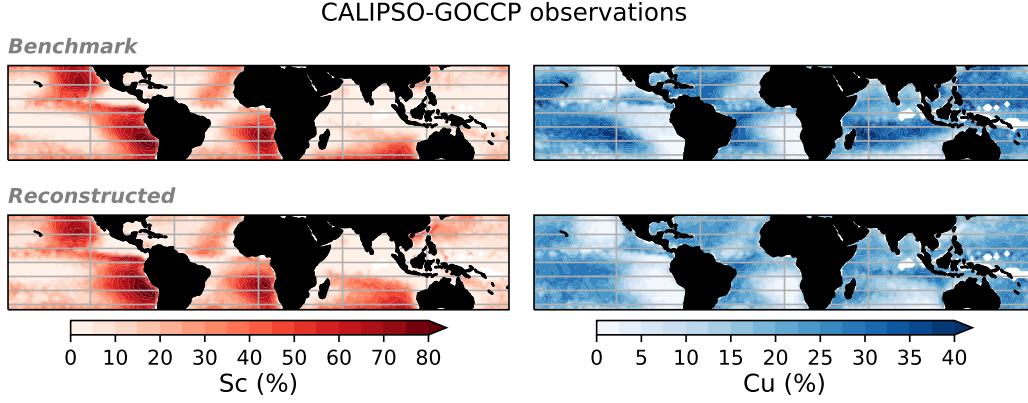
2.3.2 Categorization based on LCC

Herein we propose a new approach to discriminate Sc from Cu, which is based on cloud properties and thus alleviates the aforementioned problem. This categorization originates from the idea that overcast Sc scenarios typically have larger cloud cover than broken Cu cloud fields. In particular, we utilize the averaged LCC in tropical subsidence oceanic regions in each monthly time step to determine whether the grid box is dominated by Sc or Cu. The observed Sc- and Cu- cloud cover distributions derived from CASCCAD exhibit a crossover at this threshold. It should be noted that throughout this work we incorporate CASCCAD transitioning regimes into the Sc component, whereby their contribution to Sc cloud cover is small (Cesana et al., 2019b). This action is further justified by the fact that Sc-Cu transitioning categories ("broken Sc", "Cu under Sc", "Cu with stratiform outflow") overall show a greater resemblance to the pure Sc- than to the pure Cu-category when comparing their morphological characteristics (Cesana et al., 2019b) as well as optical properties (Pincus et al., 1999).

Figure 2 evaluates geographical distributions of Sc- and Cu-cloud cover created with the novel Sc-Cu categorization being applied to CALIPSO-GOCCP observations of LCC. The benchmark Sc- and Cu-cloud cover components are obtained from CALIPSO-GOCCP utilizing the relative frequency of occurrence (RFO) of a given cloud type derived from CASCCAD (e.g., RFO_{Sc}; whereby $RFO_{Cu} = 1 - RFO_{Sc}$) to determine whether grid box is classified as being either Sc-dominated ($RFO_{Sc} > 0.5$) or Cu-dominated ($RFO_{Sc} \leq 0.5$). Both reconstructed cloud-type distributions show a good match with their benchmark counterparts derived from CASCCAD.

Both Sc-Cu categorizations perform similarly well when applied to observational LCC dataset (Supplementary Text 1). There is indeed some ambiguity about the outcome of the two categorizations when employed in climate models. It should thereby be noted that we utilize a model-dependent LCC threshold when employing a new categorization in GCMs. We next proceed with a regime-oriented validation of CMIP6 models using the new Sc-Cu categorization (Section 3). Finally, Supplementary Text 3 briefly compares the two categorizations in models.

Figure 2. Evaluation of reconstructed cloud-type distributions obtained with novel Sc-Cu discrimination utilizing a dynamic LCC threshold, being applied to CALIPSO-GOCCP observations of LCC. Benchmark Sc- and Cu- cloud cover components are derived from CASCCAD.
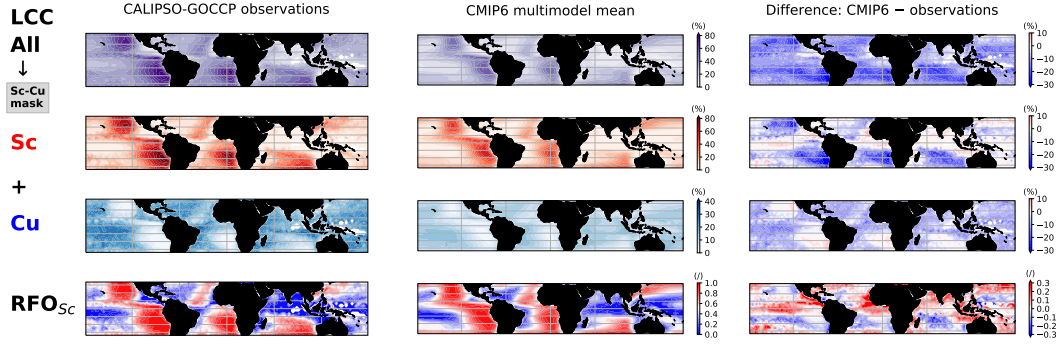
3 Results and Discussion
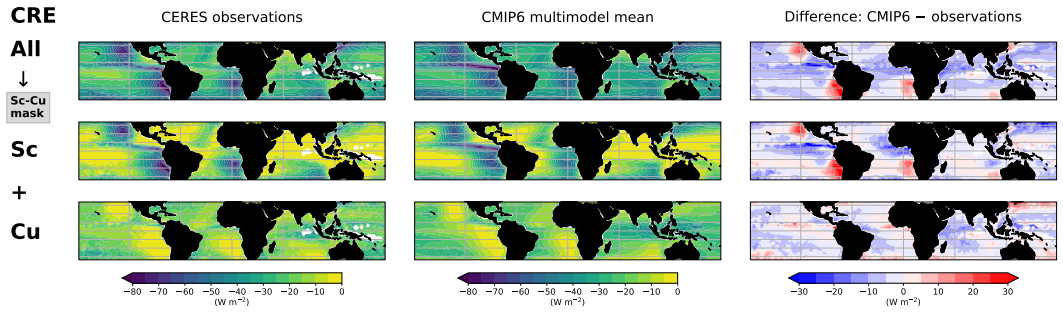
3.1 Spatial patterns of LCC and shortwave CRE

Figure 3 compares geographical distributions of low-cloud type climatology in subsidence areas of tropical oceans as simulated by the CMIP6 multimodel mean with CALIPSO-GOCCP observations. It is clear that latest climate models still struggle representing low cloudiness: on average, LCC in both Sc- and Cu-regions is strongly underestimated. The absolute bias reaches up to 30 % in Sc-regions and up to 15 % in Cu-regions. The CMIP6 models, on average, approximately capture geographical locations of the two regimes; namely stratocumulus decks off the west coast of the continents and shallow cumuli scattered further west over the open ocean. Nevertheless, the inspection of the relative frequency of occurrence of a given cloud type (e.g., RFO_{Sc}, Fig. 3; bottom row) reveals areas where models simulate inadequate amount of a particular cloud type relative to low clouds compared to observations.

Figure 4 compares the corresponding shortwave cloud-radiative effect at TOA as simulated by the CMIP6 multimodel mean with CERES observations. The negative CRE field implies a cooling effect of low clouds on climate throughout tropical oceans, although the pattern is by far not uniform. Instead, it markedly reflects the presence of individual cloud regimes: it stems predominantly from Sc-regions, whereas it is smaller in Cu-regions. The CMIP6 models, on average, overestimate the magnitude of the observed negative CRE throughout the majority of tropical oceans. Figures S3 and S4 additionally show geographical distributions of LCC and CRE decomposed into Sc- and Cu-components as simulated by individual CMIP6 models.

Figure 5 evaluates spatial patterns of simulated LCC and SW CRE against observations with the aid of Taylor diagrams (Taylor, 2001). They concurrently display multiple metrics including normalized standard deviation and spatial correlation coefficient, whereby the anomalies are computed relative to the total mean (8-year period). It is apparent that CMIP6 models struggle capturing geographical distributions of LCC and CRE in both Sc- and Cu-regions of tropical oceans. Nevertheless, the correlation coefficient between the modeled and observed field is mostly higher in Sc-regions than in Cu-regions, which is evident for both LCC and CRE. Noteworthy, all models underestimate the observed variability of LCC in both Sc- and Cu-regions, with the exception of IPSL-CM6A-LR, which is in closest agreement with observations. The variability of simulated CRE

Figure 3. Geographical distributions of low-cloud type in CALIPSO-GOCCP observations and CMIP6 multimodel mean. Bottom left and middle panels visualize RFO_{Sc}: regions shaded red are dominated by Sc, while regions shaded blue are dominated by Cu. The right column shows the corresponding difference between the CMIP6 multimodel mean and observations.
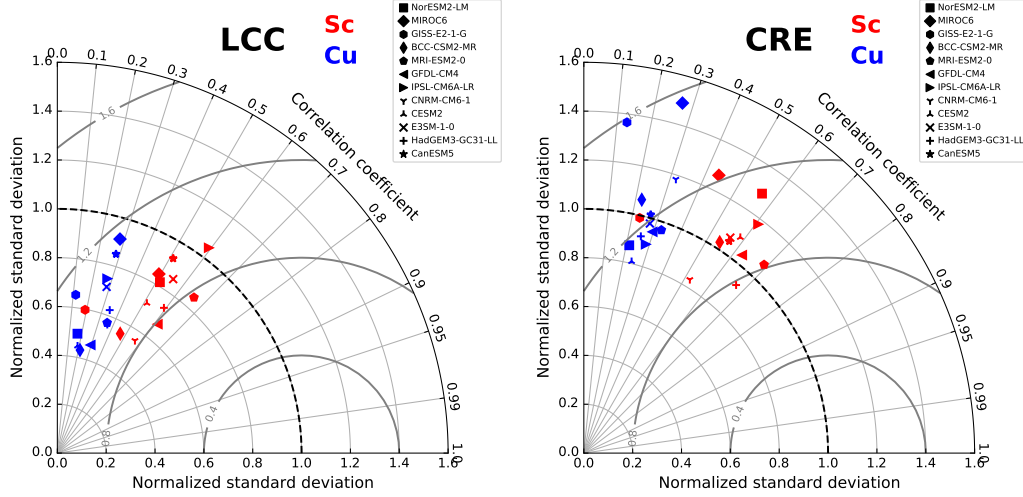

Figure 4. Geographical distributions of SW CRE associated with each low-cloud regime in CERES observations and CMIP6 multimodel mean as well as the corresponding difference.

generally shows a better match with observations, whereby normalized standard deviations commonly lie in the range between 0.8 and 1.2. The most noticeable outlier is MIROC6, which significantly overestimates the variability in both Sc- and Cu-regions. We identify further contrasting findings for Sc- and Cu-regimes, whereby models mostly underestimate the observed variability of CRE in Cu-regions, whereas they tend to overestimate it in Sc-regions. These results exemplify there are other factors than LCC which profoundly affect the CRE bias.

3.2 Relationship between LCC and shortwave CRE

Figure 6 (top) additionally displays probability density functions (PDFs) of LCC in subsidence regimes of tropical oceans. The division of the latter into Sc- and Cu-components reveals that models simulate strongly biased LCC distribution within each of the two regimes. Specifically, the observed PDF peaks at approximately 55 and 35 % within Sc- and Cu-regions, respectively. Contrarily, model PDFs generally peak in the range between 20 and 40 % in Sc-regions, whereas they predominantly peak between 5 and 30 % in Cu-regions. We further note that the shape of simulated distributions is highly variable across the CMIP6 ensemble. The best-performing model is CanESM5, which fairly
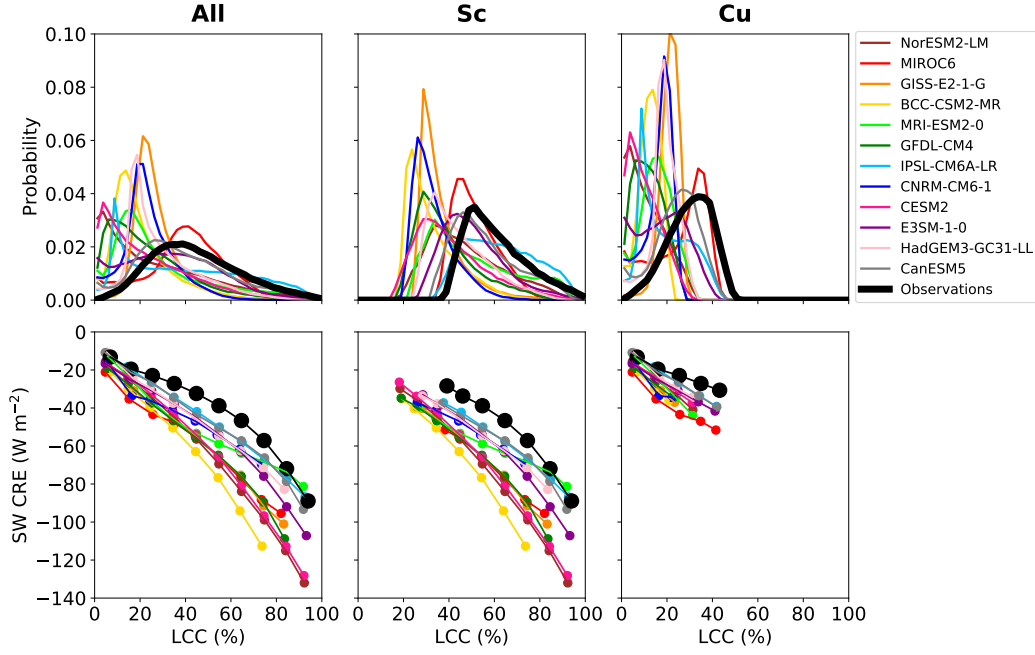
Figure 5. Taylor diagrams evaluating simulated LCC (left) and SW CRE (right) in Sc- and Cu-regions of tropical oceans.

well captures the observed distributional peak and shape in Sc- and Cu-regions. Figure S5 offers an alternative visualization of these results.

We next investigate the relationship between LCC and SW CRE shown in Fig. 6 (bottom). As expected the observed amount of reflected sunlight and hence the magnitude of negative SW CRE increases with increasing LCC. Noteworthy, the observed rate of increase is larger in Sc- than in Cu-regions. The observed nonlinear relationship between LCC and CRE is generally attributed to the increasing liquid water path with increasing LCC. Črnivec and Mayer (2019), as an illustration, investigated a shallow cumulus cloud field rising into stratocumulus and showed that both cloud cover and liquid water path concurrently increase with the simulation time.

Remarkably, all climate models overestimate the magnitude of negative SW CRE at a given LCC (by up to a factor of 2 to 3), which is evident throughout the entire range of LCC. This is consistent with findings of Nam et al. (2012) and implies that tropical low cloudiness in CMIP6 models remains too bright. The latter bias might be attributed to the inappropriate amount of averaged liquid water content, which is thus likely overestimated in models, as well as to other factors such as the parameterization of subgrid cloud variability and optical properties within the radiation scheme. CanESM5, which best captures the observed PDF of LCC, also exhibits the smallest bias in reflectance within both Sc- and Cu-regions. This is again in line with Nam et al. (2012), who pointed out that previous version of the Canadian GCM (CanAM4) incorporating proficient parameterizations of subgrid cloud structure, was the model that minimized the overestimation of negative CRE among their set of analyzed CMIP5 members. BCC-CSM2-MR exhibits the largest CRE bias in Sc-regions, while in Cu-regions MIROC6 shows the largest discrepancy from observations. Studies exploiting a rich combination of measurements (Pincus et al., 1999) and large-eddy-simulations (Črnivec and Mayer, 2020, 2021) reveal that Sc and Cu own distinct internal inhomogeneity characteristics. The contrasting heterogeneity of stratiform and convective clouds is not yet properly addressed within radiation schemes of current GCMs.

Figure 6. Top: Probability density functions of LCC derived from observations and CMIP6 models in subsidence regimes of tropical oceans as well as separately in regions dominated by Sc and Cu. Bottom: The corresponding mean 2D histograms of LCC and SW CRE.
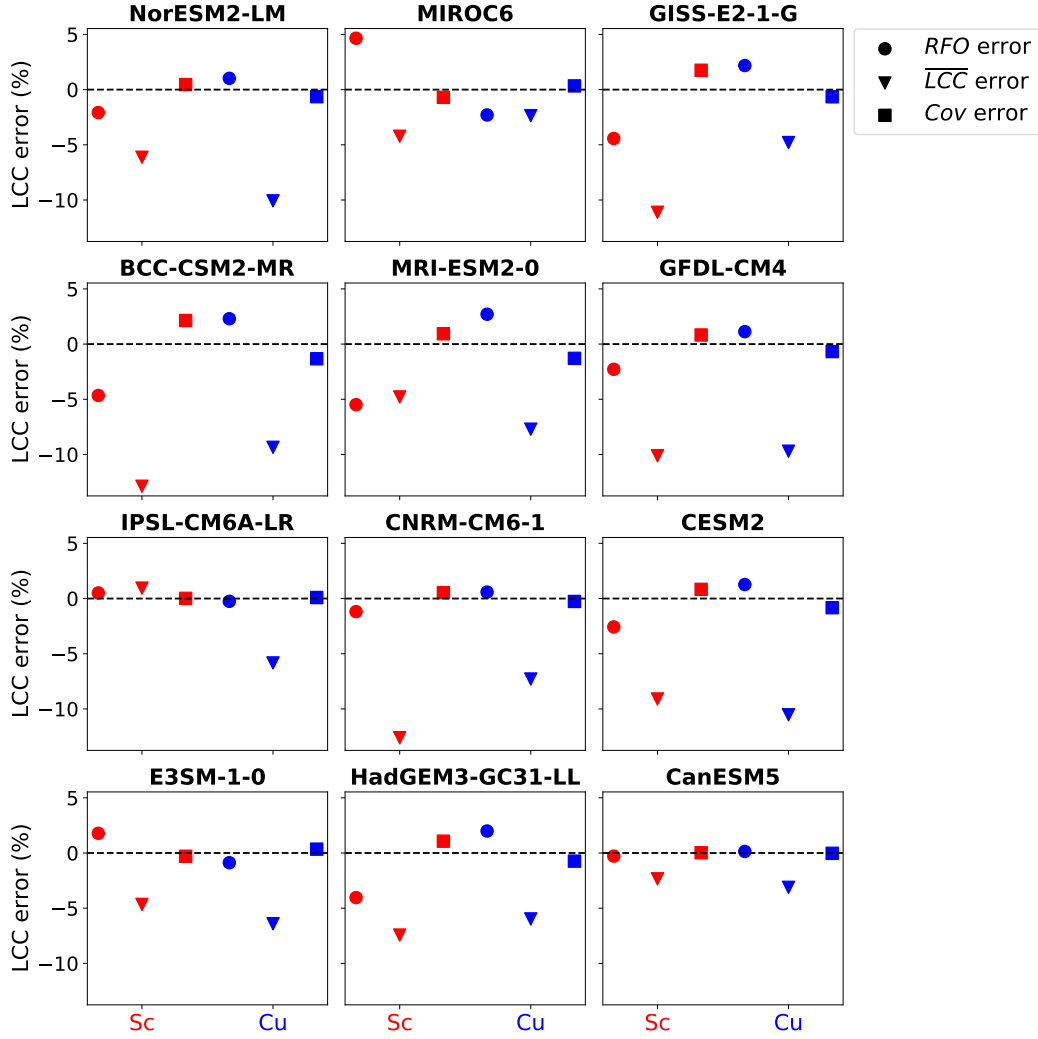
3.3 LCC error decomposition

To gain further insight into cloud biases it is convenient to decompose overall LCC model error of a specific cloud regime (r) into various components as follows (e.g., Schudeboom and McDonald, 2021):

$$\delta LCC_r = LCC_r^{obs} \Delta RFO_r + RFO_r^{obs} \Delta LCC_r + \Delta LCC_r \Delta RFO_r, \tag{1}$$

where the relative frequency of occurrence RFO_r is the rate at which given cloud regime occurs; $\Delta RFO_r = RFO_r^{mod} - RFO_r^{obs}$ and $\Delta LCC_r = LCC_r^{mod} - LCC_r^{obs}$ capture the difference between model and observations. Thus the three terms on the right-hand side of Eq. 3.3 represent the error due to RFO, the error due to mean LCC magnitude ($\overline{LCC}$) and finally the error covariance term.

Figure 7 shows results of the overall LCC error decomposition according to Eq. 3.3 within each of the two regimes (Sc, Cu), highlighting the complex nature of cloud biases among individual CMIP6 ensemble members. As anticipated the error covariance is generally small, therefore solely RFO and $\overline{LCC}$ errors are discussed in the following. Despite the fact that each model is subjected to its unique problematics, it is possible to draw several interesting conclusions.

The majority of models underestimate RFO of Sc, whereas they overestimate RFO of Cu (MRI-ESM2-0, GISS-E2-1-G, BCC-CSM2-MR, HadGEM3-GC31-LL, CESM2, GFDL-CM4, NorESM2-LM). The apparent outlier in this regard is MIROC6, which is in line with Williams and Tselioudis (2007), who showed that two previous versions of MIROC6 also considerably overestimated RFO of tropical stratocumulus and simultaneously lacked shallow cumulus regime. There are a few models where the RFO error of both Sc and Cu is essentially zero (particularly CanESM5, IPSL-CM6A-LR, CNRM-CM6-1).

Figure 7. The LCC error in subsidence areas of tropical oceans within Sc- and Cu-regions decomposed into errors stemming from RFO, $\overline{LCC}$ and covariance.

318   Remarkably, all models underestimate $\overline{LCC}$ within Sc- and Cu-regions (except IPSL-
319 CM6A-LR, which however exhibits a negligible bias in Sc-region). Climate models that
320 most strongly underestimate the mean Sc- and Cu-cloud cover are BCC-CSM2-MR, CNRM-
321 CM6-1, CESM2, GFDL-CM4, GISS-E2-1-G and NorESM2-LM. In this subset of mod-
322 els the $\overline{LCC}$ error exceeds 10 % within either of the two regimes.

323   In the following discussion we strive to provide some physical explanations for the
324 aforementioned erroneous model behavior. Climate models frequently lack the inclusion
325 of realistic moist processes within their planetary boundary layer (PBL) parameteriza-
326 tions (e.g., Cesana et al., 2019a), which affects their ability to sustain low clouds. As an
327 illustration, the problem with the lack of Sc in GISS-E2-1-G was largely resolved in the
328 next iteration of the GISS model, whereby the moist turbulence scheme of Bretherton
329 and Park (2009) was newly implemented. One should also keep in mind that the under-
330 estimation of low cloudiness can partially stem from the shielding effect of high clouds,
331 which might be overestimated in some models compared to observations, although we
332 filter subsidence regimes to minimize this problem.

The best performing model overall is CanESM5, which exhibits a zero bias in RFO and only a minor bias in $\overline{LCC}$ within both Sc- and Cu-regions. Recall that CanESM5 remarkably well matches the observed relationship between LCC and EIS (Fig. 1). The IPSL-CM6A-LR model, moreover, has a negligible error in RFO and $\overline{LCC}$ within the Sc-regime. This is in agreement with Madeleine et al. (2020) who showed that the representation of low-level clouds (and their reflectance) in the IPSL-CM6 model has considerably improved compared to the previous model version participating in CMIP5. However, it is important to bear in mind that this apparent model improvement could be a consequence of model tuning, whereby the same observational datasets of LCC and CRE employed for the present model validation were used at IPSL to adjust free model parameters in an attempt to match the observed fields of clouds and radiation (Hourdin et al., 2019). Figure 1 indeed reveals that in the IPSL-CM6A-LR model LCC grows too strongly with EIS, which acts to offset the great lack of EIS in this model, so that the LCC error is eventually small.

We furthermore revisited a question, whether the McICA noise could lead to notable LCC biases in climate models containing the McICA radiation scheme (NorESM2-LM, GFDL-CM4, CESM2, E3SM-1-0, HadGEM3-GC31-LL, CanESM5). We found no evidence that the random noise generated by McICA is responsible for a notable underestimation of LCC, which is consistent with previous work examining older generation of GCMs (e.g., Barker et al., 2008). We also found no relationship between low-cloud biases in the present-day climate and equilibrium climate sensitivity.

4 Summary and conclusions

Low clouds are ubiquitous in the tropics and intensely cool the Earth's climate, thus it is of tremendous importance to properly capture this effect in climate models. The overall objective of this study was to employ satellite observations to evaluate the representation of marine tropical stratocumulus and shallow cumulus and their impact on the Earth's radiation budget in a subset of latest climate models in the present-day climate. To that end, we first introduced a new approach to discriminate Sc from Cu based on a dynamic LCC threshold. The new Sc-Cu categorization proved to work well when applied to CALIPSO-GOCCP observations of LCC, validated against proper Sc- and Cu-components derived from the Cumulus And Stratocumulus CloudSat-CALIPSO Dataset. Compared to the traditional approach for establishing low-cloud regimes utilizing a fixed threshold of EIS, the new Sc-Cu categorization is more reliable when analyzing climate models, since the latter systematically underestimate EIS implied by multiple reanalysis datasets and generally misrepresent the relationship between EIS and LCC.

Utilizing the newly proposed Sc-Cu categorization we then assessed models' fidelity to represent Sc and Cu together with their radiative effect at the top of the atmosphere in the present-day climate. We thereby analyzed a suite of twelve state-of-the-art climate models stemming from various modeling centers participating in phase 6 of CMIP. We restricted our analysis on subsidence regimes over tropical oceans, where low clouds are not obscured by mid- and high-level clouds. We found that CMIP6 models underestimate the cloud cover in both Sc- and Cu-dominated regions of tropical oceans. A more detailed inspection of cloud biases revealed that most climate models underestimate RFO of Sc and overestimate RFO of Cu. We further showed that tropical low cloudiness in CMIP6 models remains too bright.

The results of the present study are in line with a recent work by Konsta et al. (2022), who demonstrated that low-level marine tropical clouds in six CMIP6 models are too few and too bright, but also too compact and too homogeneous. The present study extends the results of Konsta et al. (2022) by evaluating twelve CMIP6 models and by discriminating stratocumulus and shallow cumulus regimes. All in all, these findings im-

ply that contemporary climate models are still subjected to notable biases in clouds and radiation, which should fuel further climate model development.

5 Open Research

The CASCCAD dataset is available at GISS website (https://data.giss.nasa.gov/clouds/casccad/). CERES-EBAF 4.0 shortwave TOA radiative fluxes were downloaded from the CERES website (https://ceres.larc.nasa.gov/data/#energy-balanced-and-filled-ebaf). ERA5 data were downloaded from https://cds.climate.copernicus.eu/cdsapp#!/dataset/reanalysis-era5-single-levels-monthly-means?tab=form and https://cds.climate.copernicus.eu/cdsapp#!/dataset/reanalysis-era5-pressure-levels-monthly-means?tab=form. NCEP-DOE R2 data were downloaded from the NOAA ESRL Physical Sciences Division website (http://www.esrl.noaa.gov/psd/data/). The CMIP6 output was downloaded from the ESGF (https://esgf-node.llnl.gov/search/cmip6/).

References

Ackerman, A. S. and Toon, O. B.   Unrealistic desiccation of marine stratocumulus clouds by enhanced solar absorption. *Nature*, 380:512–515, 1996. doi: 10.1038/380512a0.

Ackerman, A. S., Toon, O. B., and Hobbs, P. V.   Dissipation of marine stratiform clouds and collapse of the marine boundary layer due to the depletion of cloud condensation nuclei by clouds.   *Science*, 262:226–229, 1993.   doi: 10.1126/science.262.5131.226.

Ackerman, A. S., Toon, O. B., Stevens, D. E., Heymsfield, A. J., Ramanathan, V., and Welton, E. J.   Reduction of tropical cloudiness by soot.   *Science*, 288: 1042–1047, 2000. doi: 10.1126/science.288.5468.1042.

Ackerman, A. S., van Zanten, M. C., Stevens, B., Savic-Jovcic, V., Bretherton, C. S., Chlond, A., et al.   Large-eddy simulations of a drizzling, stratocumulus-topped marine boundary layer. *Mon. Weather Rev.*, 137:1083–1110, 2009. doi: 10.1175/2008MWR2582.1.

Andrews, M. B., Ridley, J. K., Wood, R. A., Andrews, T., Blockley, E. W., Booth, B., et al.   Historical simulations with HadGEM3-GC3.1 for CMIP6.   *J. Adv. Model. Earth Syst.*, 12:e2019MS001995, 2020. doi: 10.1029/2019MS001995.

Barker, H. W., Cole, J. N. S., Morcrette, J.-J., Pincus, R., Risnen, P., von Salzen, K., and Vaillancourt, P. A.   The Monte Carlo Independent Column Approximation: an assessment using several global atmospheric models.   *Q. J. R. Meteorol. Soc.*, 134:1463–1478, 2008. doi: 10.1002/qj.303.

Bodas-Salcedo, A., Webb, M. J., Bony, S., Chepfer, H., Dufresne, J., Klein, S. A., et al.   COSP Satellite simulation software for model assessment.   *Bull. Amer. Meteorol. Soc.*, 92:1023–1043, 2011. doi: 10.1175/2011BAMS2856.1.

Bony, S. and Dufresne, J.-L. Marine boundary layer clouds at the heart of tropical cloud feedback uncertainties in climate models. *Geophys. Res. Lett.*, 32:L20806, 2005. doi: 10.1029/2005GL023851.

Bony, S., Stevens, B., Frierson, D., Jakob, C., Kageyama, M., Pincus, R., et al. Clouds, circulation and climate sensitivity. *Nat. Geosci.*, 8:261–268, 2015. doi: 10.1038/NGEO2398.

Boucher, O., Servonnat, J., Albright, A. L., Aumont, O., Balkanski, Y., Bastrikov, V., et al. Presentation and Evaluation of the IPSL-CM6A-LR Climate Model. *J. Adv. Model. Earth Syst.*, 12:e2019MS002010, 2020. doi: 10.1029/2019MS002010.

Bretherton, C. S. and Park, S. A New Moist Turbulence Parameterization in the Community Atmosphere Model. *J. Climate*, 22:3422–3448, 2009. doi: 10.1175/2008JCLI2556.1.

Cesana, G., Chepfer, H., Winker, D., Getzewich, B., Cai, X., Jourdan, O., et al. Using in situ airborne measurements to evaluate three cloud phase products derived from CALIPSO. *J. Geophys. Res. - Atmos.*, 121:5788–5808, 2016. doi: 10.1002/2015JD024334.

Cesana, G. V. and Chepfer, H. How well do climate models simulate cloud vertical structure? A comparison between CALIPSO-GOCCP satellite observations and CMIP5 models. *Geophys. Res. Lett.*, 39:L20803, 2012. doi: 10.1029/2012GL053153.

Cesana, G. V. and Del Genio, A. D. Observational constraint on cloud feedbacks suggests moderate climate sensitivity. *Nat. Clim. Change*, 11:213–218, 2021. doi: 10.1038/s41558-020-00970-y.

Cesana, G. V. and Waliser, D. E. Characterizing and understanding systematic biases in the vertical structure of clouds in CMIP5/CFMIP2 models. *Geophys. Res. Lett.*, 43:10538–10546, 2016. doi: 10.1002/2016GL070515.

Cesana, G. V., Del Genio, A. D., Ackerman, A. S., Kelley, M., Elsaesser, G., Fridlind, A. M., Cheng, Y., and Yao, M.-S. Evaluating models' response of tropical low clouds to SST forcings using CALIPSO observations. *Atmos. Chem. Phys.*, 19:2813–2832, 2019a. doi: 10.5194/acp-19-2813-2019.

Cesana, G. V., Del Genio, A. D., and Chepfer, H. The Cumulus And Stratocumulus CloudSat-CALIPSO Dataset (CASCCAD). *Earth Syst. Sci. Data*, 11:1745–1764, 2019b. doi: 10.5194/essd-11-1745-2019.

Cesana, G. V., Waliser, D. E., Henderson, D., L'Ecuyer, T. S., Jiang, X., and Li, J.-L. The vertical structure of radiative heating rates: A multimodel evaluation using A-Train satellite observations. *J. Climate*, 32:1573–1590, 2019c. doi: 10.1175/JCLI-D-17-0136.1.

Chepfer, H., Winker, D., Chiriaco, M., Dufresne, J.-L., and Seze, G. Use of CALIPSO lidar observations to evaluate the cloudiness simulated by a climate model. *Geophys. Res. Lett.*, 35:L15704, 2008. doi: 10.1029/2008GL034207.

Chepfer, H., Bony, S., Winker, D., Cesana, G. V., Dufresne, J., Minnis, P., Stubenrauch, C., and Zeng, S. The GCM-Oriented CALIPSO Cloud Product (CALIPSO-GOCCP). *J. Geophys. Res. - Atmos.*, 115:D00H16, 2010. doi: 10.1029/2009JD012251.

Danabasoglu, G., Lamarque, J.-F., Bacmeister, J., Bailey, D. A., DuVivier, A. K., Edwards, J., et al. The Community Earth System Model Version 2 (CESM2). *J. Adv. Model. Earth Syst.*, 12:e2019MS001916, 2020. doi: 10.1029/2019MS001916.

Eyring, V., Bony, S., Meehl, G. A., Senior, C. A., Stevens, B., Stouffer, R. J., and Taylor, K. E. Overview of the Coupled Model Intercomparison Project Phase 6 (CMIP6) experimental design and organization. *Geosci. Model Dev.*, 9: 1937–1958, 2016. doi: 10.5194/gmd-9-1937-2016.

Golaz, J.-C., Caldwell, P. M., Van Roekel, L. P., Petersen, M. R., Tang, Q., Wolfe, J. D., et al. The DOE E3SM Coupled Model Version 1: Overview and Evalua-

tion at Standard Resolution. *J. Adv. Model. Earth Syst.*, 11:2089–2129, 2019. doi: 10.1029/2018MS001603.

Held, I. M., Guo, H., Adcroft, A., Dunne, J. P., Horowitz, L. W., Krasting, J., et al. Structure and Performance of GFDL's CM4.0 Climate Model. *J. Adv. Model. Earth Syst.*, 11:3691–3727, 2019. doi: 10.1029/2019MS001829.

Hourdin, F., Rio, C., Grandpeix, J.-Y., Madeleine, J.-B., Cheruy, F., Rochetin, N., et al. LMDZ6A: The Atmospheric Component of the IPSL Climate Model With Improved and Better Tuned Physics. *J. Adv. Model. Earth Syst.*, 12(7): e2019MS001892, 2019. doi: 10.1029/2019MS001892.

Jiang, J. H., Su, H., Zhai, C., Perun, V. S., Del Genio, A., Nazarenko, L. S., et al. Evaluation of cloud and water vapor simulations in CMIP5 climate models using NASA "A-Train" satellite observations. *J. Geophys. Res.*, 117:D14105, 2012. doi: 10.1029/2011JD017237.

Karlsson, J., Svensson, G., and Rodhe, H. Cloud radiative forcing of subtropical low level clouds in global models. *Clim. Dyn.*, 30:779–788, 2008. doi: 10.1007/s00382-007-0322-1.

Kelley, M., Schmidt, G. A., Nazarenko, L., Bauer, S. E., Ruedy, R., Russell, G. L., et al. GISS-E2.1: Configurations and climatology. *J. Adv. Model. Earth Syst.*, 12:e2019MS002025, 2020. doi: 10.1029/2019MS002025.

Klein, S. A., Hall, A., Norris, J. R., and Pincus, R. Low-Cloud Feedbacks from Cloud-Controlling Factors: A Review. *Surv. Geophys.*, 38:13071329, 2017. doi: 10.1007/s10712-017-9433-3.

Konsta, D., Dufresne, J.-L., Chepfer, H., Vial, J., Koshiro, T., Kawai, H., et al. Low-Level Marine Tropical Clouds in Six CMIP6 Models Are Too Few, Too Bright but Also Too Compact and Too Homogeneous. *Geophys. Res. Lett.*, 49(11): e2021GL097593, 2022. doi: 10.1029/2021GL097593.

Loeb, N. G., Doelling, D. R., Wang, H., Su, W., Nguyen, C., Corbett, J. G., et al. Clouds and the Earth's Radiant Energy System (CERES) Energy Balanced and Filled (EBAF) Top-of-Atmosphere (TOA) Edition-4.0 Data Product. *J. Climate*, 31:895–918, 2018. doi: 10.1175/JCLI-D-17-0208.1.

Madeleine, J.-B., Hourdin, F., Grandpeix, J.-Y., Rio, C., Dufresne, J.-L., Vignon, E., et al. Improved Representation of Clouds in the Atmospheric Component LMDZ6A of the IPSL-CM6A Earth System Model. *J. Adv. Model. Earth Syst.*, 12(10):e2020MS002046, 2020. doi: 10.1029/2020MS002046.

Myers, T. A., Scott, R. C., Zelinka, M. D., Klein, S. A., Norris, J. R., and Caldwell, P. M. Observational constraints on low cloud feedback reduce uncertainty of climate sensitivity. *Nat. Clim. Change*, 2021. doi: 10.1038/s41558-021-01039-0.

Nam, C., Bony, S., Dufresne, J.-L., and Chepfer, H. The too few, too bright tropical low-cloud problem in CMIP5 models. *Geophys. Res. Lett.*, 39:L21801, 2012. doi: 10.1029/2012GL053421.

Pincus, R., McFarlane, S. A., and Klein, S. A. Albedo bias and the horizontal variability of clouds in subtropical marine boundary layers: Observations from ships and satellites. *J. Geophys. Res. - Atmos.*, 104:6183–6191, 1999. doi: 10.1029/1998JD200125.

Pincus, R., Barker, H. W., and Morcrette, J. J. A fast, flexible, approximate technique for computing radiative transfer in inhomogeneous cloud fields. *J. Geophys. Res. - Atmos.*, 108:4376, 2003. doi: 10.1029/2002jd003322.

Pincus, R., Batstone, C. P., Hofmann, R. J. P., Taylor, K. E., and Glecker, P. J. Evaluating the present-day simulation of clouds, precipitation, and radiation in climate models. *J. Geophys. Res. - Atmos.*, 113:D14209, 2008. doi: 10.1029/2007jd009334.

Raisanen, P., Barker, H. W., Khairoutdinov, M. F., Li, J., and Randall, D. A. Stochastic generation of subgrid-scale cloudy columns for large-scale models. *Q. J. R. Meteorol. Soc.*, 130:2047–2067, 2004. doi: 10.1256/qj.03.99.

Randall, D., Khairoutdinov, M., Arakawa, A., and Grabowski, W. Breaking the Cloud Parameterization Deadlock. *Bull. Amer. Meteorol. Soc.*, 84:1547–1564, 2003. doi: 10.1175/Bams-84-11-1547.

Schneider, T., Teixeira, J., Bretherton, C. S., Brient, F., Pressel, K. G., Schär, C., and Siebesma, A. P. Climate goals and computing the future of clouds. *Nat. Clim. Change*, 7:3–5, 2017. doi: 10.1038/nclimate3190.

Schuddeboom, A. J. and McDonald, A. J. The Southern Ocean Radiative Bias, Cloud Compensating Errors, and Equilibrium Climate Sensitivity in CMIP6 Models. *J. Geophys. Res. - Atmos.*, 126(22):e2021JD035310, 2021. doi: 10.1029/2021JD035310.

Seland, Ø., Bentsen, M., Olivié, D., Toniazzo, T., Gjermundsen, A., Graff, L. S., et al. Overview of the Norwegian Earth System Model (NorESM2) and key climate response of CMIP6 DECK, historical, and scenario simulations. *Geosci. Model Dev.*, 13:6165–6200, 2020. doi: 10.5194/gmd-13-6165-2020.

Sherwood, S., Webb, M. J., Annan, J. D., Armour, K. C., Forster, P. M., Hargreaves, J., et al. An assessment of Earth's climate sensitivity using multiple lines of evidence. *Rev. Geophys.*, 58:e2019RG000678, 2020. doi: 10.1029/2019RG000678.

Stephens, G., Winker, D., Pelon, J., Trepte, C., Vane, D., Yuhas, C., LEcuyer, T., and Lebsock, M. CloudSat and CALIPSO within the A-Train: Ten Years of Actively Observing the Earth System. *Bull. Amer. Meteorol. Soc.*, 99:569–581, 2018. doi: 10.1175/BAMS-D-16-0324.1.

Stephens, G. L., Vane, D. G., Boain, R. J., Mace, G. G., Sassen, K., Wang, Z., et al. The CloudSat mission and the A-Train: A new dimension of space-based observations of clouds and precipitation. *Bull. Amer. Meteorol. Soc.*, 83: 1771–1790, 2002. doi: 10.1175/BAMS-83-12-1771.

Stevens, B. and Bony, S. What Are Climate Models Missing? *Science*, 340:1053–1054, 2013. doi: 10.1126/science.1237554.

Stevens, B., Ackerman, A. S., Albrecht, B. A., Brown, A. R., Chlond, A., Cuxart, J., et al. Simulations of trade wind cumuli under a strong inversion. *J. Atmos. Sci.*, 58:1870–1891, 2001. doi: 10.1175/1520-0469(2001)058⟨1870: SOTWCU⟩2.0.CO;2.

Swales, D. J., Pincus, R., and Bodas-Salcedo, A. The Cloud Feedback Model Intercomparison Project Observational Simulator Package: Version 2. *Geosci. Model Dev.*, 11:77–81, 2018. doi: 10.5194/gmd-11-77-2018.

Swart, N. C., Cole, J. N. S., Kharin, V. V., Lazare, M., Scinocca, J. F., Gillett, N. P., et al. The Canadian Earth System Model version 5 (CanESM5.0.3). *Geosci. Model Dev.*, 12:4823–4873, 2019. doi: 10.5194/gmd-12-4823-2019.

Tatebe, H., Ogura, T., Nitta, T., Komuro, Y., Ogochi, K., Takemura, T., et al. Description and basic evaluation of simulated mean state, internal variability, and climate sensitivity in MIROC6. *Geosci. Model Dev.*, 12:2727–2765, 2019. doi: 10.5194/gmd-12-2727-2019.

Taylor, K. E. Summarizing multiple aspects of model performance in a single diagram. *J. Geophys. Res. - Atmos.*, 106:7183–7192, 2001. doi: 10.1029/2000JD900719.

Teixeira, J., Cardoso, S., Bonazzola, M., Cole, J., Del Genio, A., DeMott, C., et al. Tropical and sub-tropical cloud transitions in weather and climate prediction models: The GCSS/WGNE Pacific Cross-section Intercomparison (GPCI). *J. Climate*, 24:5223–5256, 2011. doi: 10.1175/2011JCLI3672.1.

Tselioudis, G., Rossow, W. B., Jakob, C., Remillard, J., Tropf, D., and Zhang, Y. Evaluation of clouds, radiation, and precipitation in CMIP6 models using global weather states derived from ISCCP-H cloud property data. *J. Climate*, 34:7311–7324, 2021. doi: 10.1175/JCLI-D-21-0076.1.

Črnivec, N. and Mayer, B. Quantifying the bias of radiative heating rates in numerical weather prediction models for shallow cumulus clouds. *Atmos. Chem.*

Phys., 19:8083–8100, 2019. doi: 10.5194/acp-19-8083-2019.

Črnivec, N. and Mayer, B. The incorporation of the Triplecloulds concept into the δ-Eddington two-stream radiation scheme: solver characterization and its application to shallow cumulus clouds. *Atmos. Chem. Phys.*, 20:10733–10755, 2020. doi: 10.5194/acp-20-10733-2020.

Črnivec, N. and Mayer, B. Towards an improved treatment of cloud–radiation interaction in weather and climate models: exploring the potential of the Triplecloulds method for various cloud types using libRadtran 2.0.4. *Geosci. Model Dev.*, 14:3663–3682, 2021. doi: 10.5194/gmd-14-3663-2021.

Voldoire, A., Saint-Martin, D., Snsi, S., Decharme, B., Alias, A., Chevallier, M., et al. Evaluation of CMIP6 DECK Experiments with CNRM-CM6-1. *J. Adv. Model. Earth Syst.*, 11:2177–2213, 2019. doi: 10.1029/2019MS001683.

Weare, B. A comparison of AMIP II model cloud layer properties with ISCCP D2 estimates. *Clim. Dyn.*, 22:281–292, 2004. doi: 10.1007/s00382-003-0374-9.

Webb, M., Senior, C., Bony, S., and Morcrette, J. J. Combining ERBE and ISCCP data to assess clouds in the Hadley Centre, ECMWF and LMD atmospheric climate models. *Clim. Dyn.*, 17:905–922, 2001. doi: 10.1007/s003820100157.

Williams, K. D. and Tselioudis, G. GCM intercomparison of global cloud regimes: Present-day evaluation and climate change response. *Clim. Dyn.*, 29:231–250, 2007. doi: 10.1007/s00382-007-0232-2.

Winker, D. M., Pelon, J., Coakley, J. A., Ackerman, S. A., Charlson, R. J., and Colarco, P. R. The CALIPSO Mission: A Global 3D View of Aerosols and Clouds. *Bull. Amer. Meteorol. Soc.*, 91:1211–1230, 2010. doi: 10.1175/2010BAMS3009.1.

Wood, R. and Bretherton, C. S. On the relationship between stratiform low cloud cover and lower-tropospheric stability. *J. Climate*, 19:6425–6432, 2006. doi: 10.1175/JCLI3988.1.

Wu, T., Lu, Y., Fang, Y., Xin, X., Li, L., Li, W., et al. The Beijing Climate Center Climate System Model (BCC-CSM): the main progress from CMIP5 to CMIP6. *Geosci. Model Dev.*, 12:1573–1600, 2019. doi: 10.5194/gmd-12-1573-2019.

Yukimoto, S., Kawai, H., Koshiro, T., Oshima, N., Yoshida, K., Urakawa, S., et al. The Meteorological Research Institute Earth System Model Version 2.0, MRI-ESM2.0: Description and Basic Evaluation of the Physical Component. *J. Meteorol. Soc. Japan*, 97:931–965, 2019. doi: 10.2151/jmsj.2019-051.